Pergamon

Geochimica et Cosmochimica Acta, Vol. 68, No. 15, pp. 3141–3155, 2004

0016-7037/04 $30.00 + .00

doi:10.1016/j.gca.2003.09.020

Biomineralization of As(V)-hydrous ferric oxyhydroxide in microbial mats of an acid-sulfate-chloride geothermal spring, Yellowstone National Park

WILLIAM P. INSKEEP,[1,*] RICHARD E. MACUR,[1] GREGORY HARRISON,[1] BENJAMIN C. BOSTICK,[2] and SCOTT FENDORF[3]

[1]Thermal Biology Institute and Department of Land Resources and Environmental Sciences, Montana State University, Bozeman, MT 59717, USA

[2]Department of Earth Sciences, Dartmouth College, Hanover, NH 03755, USA

[3]Department of Geological and Environmental Sciences, Stanford University, Stanford, CA 94305-2115, USA

(*Received June* 10, 2003; *accepted in revised form September* 22, 2003)

Abstract—Acid-sulfate-chloride (pH~3) geothermal springs in Yellowstone National Park (YNP) often contain Fe(II), As(III), and S(-II) at discharge, providing several electron donors for chemolithotrophic metabolism. The microbial populations inhabiting these environments are inextricably linked with geochemical processes controlling the behavior of As and Fe. Consequently, the objectives of the current study were to (i) characterize Fe-rich microbial mats of an ASC thermal spring, (ii) evaluate the composition and structure of As-rich hydrous ferric oxides (HFO) associated with these mats, and (iii) identify microorganisms that are potentially responsible for mat formation via the oxidation of Fe(II) and or As(III). Aqueous and solid phase mat samples obtained from a spring in Norris Basin, YNP (YNP Thermal Inventory NHSP35) were analyzed using a complement of chemical, microscopic and spectroscopic techniques. In addition, molecular analysis (16S rDNA) was used to identify potentially dominant microbial populations within different mat locations. The biomineralization of As-rich HFO occurs in the presence of nearly equimolar aqueous As(III) and As(V) (~12 μM), and ~ 48 μM Fe(II), forming sheaths external to microbial cell walls. These solid phases were found to be poorly ordered nanocrystalline HFO containing mole ratios of As(V):Fe(III) of 0.62 ± 0.02. The bonding environment of As(V) and Fe(III) is consistent with adsorption of arsenate on edge and corner positions of Fe(III)-OH octahedra. Numerous archaeal and bacterial sequences were identified (with no closely related cultured relatives), along with several 16S sequences that are closely related to *Acidimicrobium, Thiomonas, Metallosphaera* and *Marinithermus* isolates. Several of these cultured relatives have been implicated in Fe(II) and or As(III) oxidation in other low pH, high Fe, and high As environments (e.g. acid-mine drainage). The unique composition and morphologies of the biomineralized phases may be useful as modern-day analogs for identifying microbial life in past Fe-As rich environments.

1. INTRODUCTION

The biomineralization of Fe(III) solid phases is a common occurrence in natural systems where aqueous Fe(II) can serve as an electron donor for chemolithotrophic metabolism, or where microbial cells serve as nucleation sites for the oxidation and or precipitation of Fe(III) minerals (see reviews by Ghiorse, 1984; Konhauser, 1998). Many Fe(II) oxidizing microorganisms including the well characterized *Acidithiobacillus ferroxidans* and *Leptothrix* sp. produce Fe(III) sheaths and can be responsible for the production of copious amounts of Fe(III) mineral phases in the surrounding environment, in part due to the large amount of Fe(II) oxidation necessary to derive energy for growth (Ehrlich, 1990). The biomineralization of hydrous Fe(III) oxides (HFO) can be accompanied by incorporation of other dissolved constituents including Si (Ferris et al., 1986; Konhauser and Ferris, 1996), Ca and PO_4 (Karl et al., 1988), SO_4 (Clarke et al., 1997), and AsO_4 (LeBlanc et al., 1996; Langner et al., 2001). The composition of biomineralized Fe(III) phases is in part a function of the concentrations of dissolved constituents present in a given environment and their tendency to adsorb onto HFO surfaces. Consequently, the pH dependence of ion specific surface complexation reactions also plays an important role in the resulting composition of biomineralized Fe(III) phases. The composition of Fe(III) phases may also be influenced by organism specific metabolic pathways, which contribute to defining the chemistry of the cell wall-aqueous interface and the environment in which nucleation and particle growth occur (Konhauser, 1998). Thus, biologic mineralization plays an important role in ion retention, and the resulting solid phases may exhibit unique signatures characteristic of their biotic origin.

There is considerable interest in the nature of arsenate [As(V)] and arsenite [As(III)] surface complexes on HFO and other Fe oxide phases, in part due to the fact that Fe oxide phases play a pivotal role in the behavior of As in natural water systems. Arsenate and arsenite are both strongly complexed by HFO and well-crystalline Fe oxides, however, the pH dependence varies for each species (Manning et al., 1998; Raven et al., 1998; Sun and Doner, 1998). Binuclear bidentate surface complexation of arsenite has been shown to be important over a broad pH range from 4 to 10, but adsorption peaks near the pKa of $H_3AsO_3^o$ = 9.23. Similar bidentate binuclear sorption mechanisms have been elucidated for arsenate, but arsenate surface complexation is favored at low pH and decreases with increasing pH (Manning et al., 1998; Sun and Doner, 1998). The commonly observed increase in solubility of As under reduced conditions is now attributed primarily to the reductive dissolution of Fe (III) oxide phases and the subsequent release

* Author to whom correspondence should be addressed (binskeep@montana.edu).

of sorbed As (Cummings et al., 1999; Zobrist et al., 2000). Iron reduction also is the suspected cause of elevated As concentrations in aquifers of Bangladesh, which has resulted in a national water quality crisis affecting millions of residents (MacArthur et al., 2001).

In acid mine drainage and geothermal environments, the co-occurrence of Fe and As can lead to the formation of HFO containing significant amounts of As, either as As(III) or As(V) (Langner et al., 2001; Morin et al., 2003). Naturally occurring HFOs containing up to 0.2 mol As per mole Fe (As:Fe) have been observed in marine hydrothermal vents (Pichler et al., 1999; Rancourt et al., 2001), and As:Fe mole ratios of 0.45 to 0.72 have been reported in HFO phases formed in acid mine drainage environments (Leblanc et al., 1996; Morin et al., 2003). Previous work on Fe microbial mats of acid-sulfate-chloride geothermal springs in Yellowstone National Park (YNP), WY, USA has also documented As:Fe ratios of 0.7 (Langner et al., 2001). Values of 0.7 approach upper limits observed for synthetic coprecipitates of As(V)-HFO phases studied by Waychunas et al. (1993) and Carlson et al. (2002). Whether synthetic or natural, the coprecipitation of high As(V)-HFOs generally results in disordered nanophases due to the high frequency of arsenate surface complexes and the resulting inhibition of further Fe-OH polymerization and oxide crystal growth (Manceau, 1995; Rancourt et al., 2001). The formation and subsequent behavior of these solid phases has important implications for As sequestration and or release in watersheds and or aquifers contaminated with As. Furthermore, the unique chemical and physical signature of these biomineralized phases represent modern-day stromatolites, which could potentially be preserved during sedimentation and consolidation to result in a fossil record of microorganisms inhabiting acidic As-Fe rich environments. Ferris et al. (1986) suggested this possibility regarding biomineralized Si-Fe rich sheaths forming on microorganisms present in geothermal sediments of YNP.

In many cases, the formation of high As(V)-HFOs is mediated by the combined microbial oxidation of As(III) and Fe(II). For example, Morin et al. (2003) recently documented the bacterial formation of As(V)-Fe(III) gels in acid mine drainage, which was likely due to the combined metabolic activity of *Acidithiobacillus ferroxidans* (Fe(II) oxidation) and *Thiomonas* sp. (As(III) oxidation). Other recent work in geothermal environments has documented rapid microbial oxidation of As(III) present in geothermal discharge waters (Gihring et al., 2001; Langner et al., 2001) or in streams down gradient from geothermal discharge (Wilkie and Hering, 1998). Pure cultures of microorganisms from each of these locations have been implicated as contributors to the observed As(III) oxidation (Gihring et al., 2001; Salmassi et al., 2002; Donahoe-Christiansen et al., 2004). In previous studies on an acid-sulfate-chloride (ASC) geothermal spring in YNP, Langner et al. (2001) and Jackson et al. (2001) described the formation of As(V)-HFO microbial mats and the associated microbial diversity using 16S rDNA analysis. The objectives of the current study were to (i) characterize Fe-rich microbial mats of an ASC thermal spring that form as a result of oxidation and biomineralization of geothermal Fe(II), (ii) evaluate in greater detail the composition and structure of high As(V)-HFO phases associated with these mats, and (iii) identify microorganisms that are either associated with and or potentially responsible for mat formation via the oxidation of Fe(II) and or As(III). To accomplish these objectives, a complement of aqueous geochemical, microscopic, spectroscopic, and surface analytical techniques were employed to characterize the Fe solid phases. In addition, molecular analysis (16S rDNA) of microbial mat samples at different locations within the Fe depositional zone was used to assess the variation in dominant 16S rDNA sequences distributed across different mat locations and to identify microbial populations with a potential role in Fe(II) and or As(III) oxidation.

2. MATERIALS AND METHODS

2.1. Site Characterization

The Hundred Springs Plain of Norris Geyser Basin contains several different types of acid-sulfate-chloride (ASC) springs, and our work has focused on low discharge acidic springs containing Fe(II), As(III), S(-II,0) and H_2 as electron donors driving primary microbial production. The data discussed in this study was obtained from an ASC geothermal spring (Fig. 1) located just south of Cinder Pool unofficially referred to as Beowulf Spring (YNP Thermal Inventory NHSP35; No. 44°43′53.4″N latitude, 110°42′40.9″ W longitude). This spring has also been the subject of U.S. Geological Survey inventory sampling as part of a larger effort to characterize the water chemistry and hydrogeology of numerous geothermal features in YNP (Ball et al., 2002). The subject spring exhibits source waters with temperatures ranging from 75–82°C and a flow rate of approximately 50 L/min. Flow rates have been observed to vary considerably (estimate 50%) across the last 2 yr, similar to seasonal fluctuations of geothermal discharge described by Fournier (1989). Beowulf Spring is similar to an adjacent (<50 m) ASC spring described in recent studies (Jackson et al., 2001; Langner et al., 2001); however, the Fe mats in Beowulf are considerably thicker (2–4 cm) and more extensive, forming extensive terraces extending nearly 10 m down gradient from discharge. Aqueous and solid phase samples were collected several times during 2001–2002 for detailed chemical characterization and molecular analyses to identify microbial populations (16S rDNA sequence analysis) present in the Fe(III)-oxyhydroxide microbial mats.

2.2. Aqueous Geochemistry

Aqueous samples were collected as a function of distance from spring discharge in October 2001, June 2002, and October 2002, filtered on site and analyzed in the Soil Analytical Laboratory (Montana State University) using inductively coupled plasma spectrometry (ICP) for major ions including Ca, Mg, Na, K, Si, Al, As, Fe and B, and trace elements including Cd, Cr, Cu, Mn, Ni, Pb, Sb, Se, and Zn. Aqueous NH_4 was determined with a flow injection analyzer using the phenolate colorimetric ($A_{630\ nm}$) procedure (APHA, 1998a). In addition, aqueous samples were analyzed on site for (i) Fe(II)/Fe(III) using the ferrozine method (To et al., 1999) employing a 5 mL filtered (0.2 μm) sample, (ii) H_2S(aq) using the amine sulfuric acid method (APHA, 1998b) employing a 7.5 mL unfiltered sample (to avoid rapid degassing of H_2S upon filtration), and (iii) predominant inorganic anions (F^-, Cl^-, SO_4^{2-}, NO_3^-, CO_3^{2-}, S_2O_3, AsO_4^{3-}) using ion chromatography (IC) employing a 25 μL injection volume, a 0.1 mol/L NaOH eluent at 1 mL/min and a Dionex AS16−4 mm ion exchange column (Dionex Corp., Sunnyvale, CA). Arsenate [As(V)] was determined using IC on an untreated sample within 30 min of sampling and on another sample treated with 10 mol/L $KMnO_4$ and conc. HCl to oxidize As(III) to As(V). The total As values determined with IC were cross-checked against total As values determined with ICP, and found to be within 10%. The amount of aqueous As(III) was calculated as the difference between arsenate As(V) and total soluble As (As_{TS}). Control samples evaluated in the laboratory confirmed efficient oxidation of As(III) using $KMnO_4$ at low pH. Aqueous pH and temperature values were obtained on site using a Mettler-Toledo portable ion meter (MA130) equipped with a temperature probe, where pH 1.68 and 4.01 buffers were calibrated at spring temperatures.

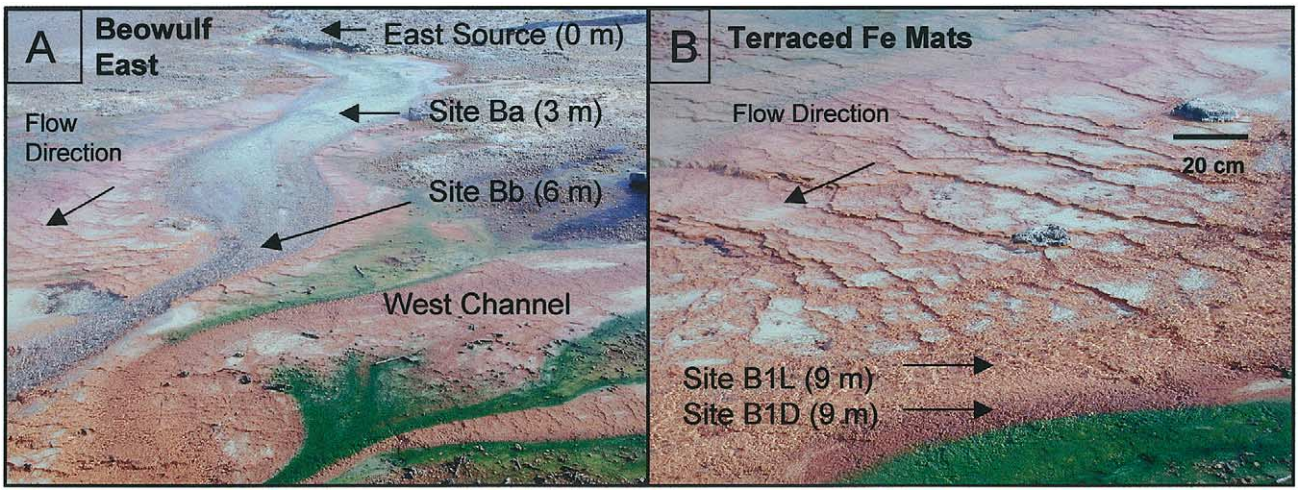

Fig. 1. Beowulf Spring located in Norris Geyser Basin, Yellowstone National Park, showing the east geothermal source (0 m) and aqueous sampling points Ba (3 m) and Bb (6 m) (A), and a view down gradient from (A) showing Fe microbial mats at sampling sites B1L (9 m) and B1D (9 m) (B). A 50–51°C isotherm is defined by the interface of Fe mats and an acid-tolerant algae, likely *Cyanidium caldarium*. Photograph taken in March 2002.

2.3. Solid Phase Characterization

Solid phase Fe mat samples were collected at a total of four locations including three from the main east channel (B1L = 9 m from east source discharge, B2 = 13 m from east source discharge, B3 = 17 m from east source discharge) and one at the terminus of the west channel as it merges with the larger east channel (B1D) during three different sampling trips (October 2001, March 2002 and June 2002). The samples were placed in sterile 50 mL tubes, transported to the laboratory within 12 h of collection, and characterized using a compliment of chemical, microscopic and spectroscopic analytical tools. Solid phase Fe mat samples were dried at 105°C for 48 h and analyzed for total ion chemistry using a HNO_3-$HClO_4$-HF acid digestion at 110°C, followed by elemental analysis using ICP. The amount of extractable Fe and As was determined using the NH_4-oxalate procedure at pH 3 on 0.1 g subsamples shaken in the dark for 2 h (Loeppert and Inskeep, 1996), followed by analysis of Fe and As using ICP. Total organic C (TOC) and total organic N (TON) were determined using a LECO furnace. Surface areas of dried and disaggregated Fe mat samples were determined using a triple point N_2(g)-BET adsorption isotherm (Micromeritics FlowSorb II 2300, Norcross, GA).

Selected brown mat samples were fixed with 3% glutaraldehyde immediately after removal from the spring. Samples were then embedded in 2% noble agar, refixed in glutaraldehyde, dehydrated in an ethanol series, and treated with propylene oxide before infiltration with Spurr's epoxy resin (Spurr, 1969). Thin sections were placed on 300 mesh copper grids and analyzed by transmission electron microscopy (TEM) using a LEO 912AB (LEO Electron Microscopy Inc., Thornwood, NY) equipped with an in-column OMEGA-type imaging spectrometer and controlled with Soft Imaging System software (Lakewood, CO). TEM images, parallel electron energy loss spectra (PEELS), electron spectroscopic images (ESI), and selected area diffraction images were acquired at an energy of 100 keV. Iron and As elemental maps were generated using energy loss spectra for the Fe-$L_{2,3}$ (708 eV) and As-$L_{2,3}$ (1323 eV) edges fitted to a three-window power law (15 eV windows).

Iron-rich microbial mat samples were also analyzed using X-ray absorption near edge structure (XANES) spectroscopy, extended X-ray absorption fine structure (EXAFS) spectroscopy and X-ray diffraction (XRD) using a synchrotron light source at the Stanford Radiation Laboratory (SSRL). Powder diffraction measurements were carried out on beamline 2–1 (SSRL) equipped with Soller slits and a diode detector. The incident energy, as well as sample and detector orientation was calibrated by performing a Rietveldt refinement on a LaB_6 thin film, which has a known and well-defined structure. The incident energy was determined to be 1.24127 Å using this method. Diffraction patterns of moist samples were collected by filling a trough in a flat, Al sample holder and covering the sample with Kapton (an amorphous, X-ray transparent film) to prevent desiccation during data collection. Data was collected in rocking mode (± 1 degree) from 5 to 60° 2θ with data points every 0.002° 2θ.

Iron and As K-edge X-ray absorption spectroscopy was performed at SSRL on beamline 4–1 using an unfocused beam detuned approximately 50% to eliminate higher order harmonics. The transmitted energies were monitored using N_2-filled ionization chambers, the fluorescence yield was determined using a Stern-Heald type fluorescence detector equipped with 6 μx filters (Ge for As, Mn for Fe Spectra were obtained from about −200 to +1000 eV about the adsorption edge of Fe and As). To avoid self-absorption phenomena, the samples were dispersed and a thin film of solid phase was mounted on a polycarbonate membrane so that the change in optical density across the Fe K-edge was less than 0.1 U. Fluorescence spectra were then compared to transmission data to confirm that self-absorption dampening was eliminated. Arsenic X-ray absorption near edge structure (XANES) spectra of normalized spectra were compared to model compounds including scorodite ($FeAsO_4 \cdot 2H_2O$), sodium arsenate, sodium arsenite, orpiment (As_2S_3), and arsenopyrite (FeAsS). Linear combination fitting of experimental XANES spectra with those of the reference materials was used to quantify As oxidation state in the samples.

The extended X-ray absorption fine structure (EXAFS) spectral region was used to determine the local coordination environment of Fe and As in the Fe-rich precipitates. For EXAFS analysis, the energy (eV) scale of normalized spectra was transformed to k-range using 11867 eV as the energy of the As K edge (E_0). Spectra were then fit with a six-point cubic spline function above the edge that followed the envelope of the decaying EXAFS spectrum (the χ(k) function). The χ(k) spectrum was then isolated and weighted by k^3 to amplify the upper k-range and Fourier-transformed without smoothing to produce a radial structure function (RSF) using a k-range of approximately 3 to 14 $Å^{-1}$. Distinct shells of the RSF function were then back-transformed to isolate the spectral contributions of each atomic shell. WinXAS was used to determine the element (Z), coordination number (CN), distance (R), and the Debye-Waller factor (σ^2, an expression of disorder) for each shell, using phase and amplitude functions using FEFF 7.02 (Zabinsky et al., 1995). Final fits were completed using unfiltered, k-weighted χ(k) spectra. Interatomic distances are typically determined within 0.02 Å and the coordination number within 30% for the first shell. Elements of similar atomic number (Z ± 2) cannot be distinguished due to similarities in the phase and amplitude functions,

although differences in local structure (i.e., interatomic distances) may help to determine backscattering elements.

2.4. DNA Extraction, Amplification and Sequence Analysis

Iron microbial mat samples were obtained on June 6, 2002, using DNA-free spatulas, placed on dry ice and transported within 8 h to a −80°C freezer before DNA extraction and partial 16S rDNA sequence analysis. The subset of samples obtained for molecular analysis included four samples from the main channel (B1L = lighter orange rust (5YR 5/8) Fe mats at 64°C; B2 = similar Fe mats in the main channel at 60–62°C, where B2T refers to the top 2 mm of mat, B2B refers to the bottom 2 mm of mat and B2C refers to a mat composite), and one sample from the terminus of the west channel at the confluence with the east channel (B1D = darker red brown (2.5YR 4/4) mats at 53°C. Sample B1D is essentially adjacent to and within 5–10 cm of sample B1L (Fig. 1B). The small but potentially significant changes in aqueous chemistry and temperature across these locations reflect gradients that yield visually and physically different types of Fe(III)-oxyhydroxide mats. The mats of the main channel near B1L are also considerably thicker and softer (up to 5 cm in some terraces, Fig. 1B) than adjacent mats at B1D, which typically range from 2 to 3 mm forming brittle platelets. In a first attempt to describe these microbial communities, we have performed a fairly thorough analysis of 16S rDNA sequences present across some of the observed mat variability to address the hypothesis that adapted microbial populations are distributed across gradients of temperature and or aqueous chemistry, and that the spatial distribution may in part be reflected in obvious variables such as mat color, thickness and texture. While molecular results from the current study will not provide definitive functional assignments to the important populations represented, we can gain significant insight regarding the potential importance of specific populations and the patterning of sequence diversity across gradients, as well as identify target sequences for complimentary and more quantitative molecular techniques including FISH, and real-time PCR.

Total DNA extracts of brown mat samples were obtained using the FastDNA SPIN Kit for Soil (Q-Biogene, Carlsbad, CA). Selected samples were evaluated before and after extraction with NH_4-oxalate (pH 3) to remove the Fe rich sheaths. The 16S rRNA genes of bacteria and archaea present in the DNA extracts were amplified by polymerase chain reaction **(**PCR) using two primer sets. One set was designed to amplify a 322 bp segment within the domain *Bacteria* using Bac1070 forward coupled with Univ1392 reverse-GC (Jackson et al., 2001). The reverse primer incorporated a 40 bp GC-rich clamp to facilitate analysis by denaturing gradient gel electrophoresis (DGGE; Ferris et al., 1996). The domain *Archaea* was targeted with a second primer set designed to amplify a 461 bp region. The forward primer was Arc931 and the reverse primer was the same Univ1392 reverse-GC described above (Jackson et al., 2001). The PCR mixtures (50 μL) contained 4.0 mM $MgCl_2$, 50 mM KCl, 10 mM Tris-HCl (pH 8), 0.1% Triton X-100, 800 μM dNTPs, 0.5 μM of each primer, 1.25 U *Taq* DNA polymerase (Promega, Madison, WI), and 1–5 μL template DNA (2–20 ng). Thermal cycler settings were 94°C for 4 min, 25–35 cycles of 94°C, 54°C and 72°C each for 55 s, and a final 7 min extension period at 72°C. To insure PCR product purity, negative control reactions (no template) were routinely performed.

PCR amplified 16S rDNA fragments were separated using denaturing gradient gel electrophoresis (DGGE) following a method modified from Ferris et al. (1996). DNA was loaded onto gels consisting of 8% acrylamide and a 40–70% denaturing gradient of urea/formamide and electrophoresed at 60 V at 60°C for 17 h using a DCode System (Bio-Rad, Hercules, CA). Gels were stained with SYBR Green II (Molecular Probes, Eugene, OR) for 30 min before photography using UV transillumination. DGGE bands of interest were prepared for sequencing by sampling with a pipet tip, rinsing the tip with PCR-grade water, and subjecting the solution to PCR as described above. The purity and identity of PCR product was checked using DGGE. The resultant DNA was purified using a Microcon filter kit (Millipore Corp. Bedford, MA) and sequenced using the same primers with exception to the 1392 reverse which did not contain a GC clamp. Sequencing reactions were performed using the ABI Prism BigDye Terminator Cycle Sequencing Ready Reaction Kit (Perkin-Elmer, Foster City, CA) and products were analyzed with an ABI Prism 310 capillary sequencer (Perkin-Elmer). Sequences were aligned and edited using Sequencher 3.1.1 software (Gene Codes Corporation, Ann Arbor, MI) and compared with sequences found in the GenBank database using BLAST (Altschul et al., 1997).

Table 1. Aqueous chemistry of geothermal discharge sampled from the predominant east source (73.7°C) of Beowulf Spring on June 6, 2002.

Cations/Anions (μM)		Primary cations/anions (μM)	
Na^+	12957	Si	4690
K^+	1258	DIC[b]	1850
Ca	135	B	717
Al	145	As	23.9
Fe	49.3	NH_4^+	79.4
Mg	8.2	DOC[c]	53
Zn	1.4	H_2S(aq)	78.7
Mn	0.73	P	4.5
Cl^-	13770	Se	2.5
SO_4^{2-}	1510	H_2 (aq)	0.02
F^-	147	Charge difference	0.9%
NO_3^-	20	Ionic strength	17.5 mM

[a] Undetected trace elements and method detection limits: Se (<4 μM); Ni, (<0.9 μM); Sb, Pb, Cr (<0.6 μM); Cd, Cu, (<0.2 μM).
[b] Dissolved inorganic C.
[c] Dissolved organic C.
[d] Charge difference and ionic strength calculated using Visual MINTEQ (Allison et al., 1991).

3. RESULTS AND DISCUSSION

3.1. Overview of Spring Chemistry and Predominant Biogeochemical Processes

The source waters of Beowulf Spring emerge from at least two locations, described here as a predominant east source (74°C) and a west source (69°C), which join approximately 9 m down gradient from each source (Fig. 1). The major ion chemistry for each of these contributing sources was characterized on two different dates and found to be within 15% of one another across all dissolved constituents. Consequently, the source water chemistry presented in Table 1 corresponds to the predominant east discharge channel sampled in June 2002. These springs are dominated by Na (13 mM), Cl (15 mM) and SO_4 (1.5 mM), but also contain significant concentrations of dissolved inorganic C (~2.5 mM), B (0.7 mM), H_2S(aq) (80 μM), NH_4 (70 μM), Fe(II) (50 μM) and As(III) (24 μM). The concentrations of nearly all constituents are similar to an adjacent ASC spring (YNP Spring Inventory No. NHSP106) studied previously containing 63 μM H_2S, 60 μM Fe(II) and 33 μM As (Langner et al., 2001).

Concentrations of several aqueous inorganic constituents change dramatically as a function of distance from geothermal discharge. Predominant changes include a decrease in H_2S(aq) from near 80 μM to less than 6 μM at sampling site B1L (9 m) and to less than 2 μM at sampling site B3 (17 m). In the west channel, a similar pattern was observed but H_2S levels declined from ~80 μM at the source to 0.3 μM at sampling site B1D. The rapid decline in H_2S(aq) across these spring intervals is likely due to both degassing of H_2S and to oxidation and precipitation of elemental S in the first 0–3 m down gradient from discharge (Xu et al., 1998). The concentration of total soluble Fe remains nearly constant at 45–48 μM from east source to sampling site B3, despite the significant accumulation

Table 2. Site descriptions and measurements of aqueous temperature, pH, total sulfide, As, and Fe in Beowulf Spring, averaged in most cases across several sampling dates in 2001–2002 to provide an indication of seasonal variation of geochemical parameters.

Site	Distance from source[a]	Description	Temperature (°C)	pH[c]	S(−II) (μM)	As(V)/As^{d}_{TS}	Fe_{TS} (μM)	Fe(II)/Fe^{e}_{TS}
West Source	0 m	Discharge	69 (3)[b]	2.98–3.05	82.3 (6.4)	0	41	0.91
East Source	0 m	Discharge	74 (4)	3.03–3.09	80.0 (5.6)	0.04 (0.05)	48 (0.5)	0.94 (0.05)
Ba	3 m	Middle of S depositional zone	71 (3)	3.01–3.14	30.4 (4.0)	0.07 (0.00)	48 (2)	0.92 (0.10)
Bb	6 m	End of S depositional zone	68 (3)	3.00–3.13	10.3 (3.2)	0.17 (0.02)	50 (3)	0.91 (0.04)
B1 Light	9 m	Early Fe depositional zone, east channel (2–4 cm thick 5YR 5/8 mats)[f]	64 (1)	2.97–3.10	4.6 (1.6)	0.32 (0.12)	49 (5.6)	0.93 (0.07)
B1 Dark	9 m	Fe depositional zone at terminus of west channel (0.2–0.4 cm thick 2.5YR 4/4 mats)	53 (1)	2.95–3.05	0.3	0.62	35	0.61
B2	13 m	Fe depositional zone, main channel (2–4 cm thick 5YR 5/8 mats)	59 (2)	2.96–3.05	2.5 (1.2)	0.41 (0.08)	46 (6)	0.94 (0.04)
B3	17 m	Fe depositional zone, main channel (2–4 cm thick 5YR 5/8 mats)	56 (2)	2.95–3.05	1.7 (0.4)	0.60 (0.19)	45 (9)	0.87 (0.01)

[a] Distances are m from predominant east source or from west source for B1 Dark.
[b] Where present, values in parentheses are standard deviations of three sampling dates.
[c] pH range given rather than means.
[d] Ratio of As(V)/As_{TS}, where As_{TS} = 24.1 (1.7) μM across all sampling positions and dates.
[e] Ratio of Fe(II)/Fe_{TS}.
[f] Munsell color of wet sample: YR = hue, followed by value/chroma.

of Fe(III) in microbial mats commencing at approximately 8 m, just upstream from sampling site B1L. Furthermore, the predominant valence of aqueous phase Fe remains as Fe(II) from east discharge to sampling site B3, despite the obvious Fe oxidation occurring to form Fe(III) solid phases that dominate the mat composition. In the west source, noticeable aqueous Fe oxidation and small decreases in total soluble Fe were observed at sampling site B1D.

Arsenite [As(III)] is the predominant form of inorganic As in Beowulf source waters, however, As(III) is oxidized down gradient from discharge, especially after concentrations of dissolved sulfide drop below 10 μM (Table 2). By the time source waters have reached sites B1, B2 and B3, approximately 30–50% of the As(III) has been oxidized to As(V). The oxidation of aqueous As(III) is inversely related to dissolved sulfide, and As(V) concentrations continue to increase significantly as spring waters flow across the Fe-rich microbial mats. Previous work in a similar ASC spring has documented that the rapid As(III) oxidation rate occurring across Fe rich mats is a direct result of biotic activity (Langner et al., 2001). Furthermore, a *Hydrogenobaculum*-like microorganism recently isolated from a similar ASC spring has been shown to oxidize As(III) (Donahoe-Christiansen et al., 2004). A detailed assessment of all possible organisms contributing to As(III) oxidation has not been accomplished, but is part of our longer term goal to fully describe organisms responsible for As transformation. The mechanisms of microbial As(III) oxidation are also not entirely clear, but it is likely that several microbial populations are involved in the oxidation of As(III) (discussion to follow), either utilizing As(III) as an electron donor for growth or oxidizing As(III) as part of a detoxification strategy (Anderson et al., 1992; Inskeep et al., 2002). Recent work completed in a nearby (~200 m) ASC spring containing 80 μM As(III) in geothermal source waters has shown that significant As(III) oxidation can occur before formation of the Fe rich mat, however, oxidation of As(III) continues to increase as the Fe mats develop (Macur, 2004). Consequently, it is likely that several adapted microbial populations play a role in the oxidation of As(III) measured down gradient from discharge. As will be discussed below, the microbial oxidation of As(III) to As(V) plays an important role in defining the formation and composition of Fe mats.

The geothermal source waters of Beowulf Spring also contain H_2CO_3 levels of at least 2 mM (Table 1). Previous measurements of DIC at an adjacent ASC spring were as high as 4.4 mM at the source. The lower concentrations of DIC in Beowulf source waters may reflect a greater loss of CO_2(g) due to outgassing before sample injection into the ion chromatograph. The prior measurements were made by titration of closed headspace samples. Although the concentration of DIC declines rapidly down gradient due to degassing, there is a significant quantity of aqueous CO_2 available for autotrophic growth and the geothermal waters are still supersaturated with respect to atmospheric CO_2 as they flow across the Fe rich mats. Concentrations of DIC in aqueous samples analyzed using ion chromatography over a 1-yr period have ranged from 0.1–0.3 mM at sampling site B2. While the concentrations of DIC in source waters of Beowulf are considerably greater than concentrations of dissolved organic C (DOC) (0.05 mM), the amount of DOC may still be important for heterotrophic growth.

3.2. Solid Phase Characterization: Fe(III)-As(V) Oxyhydroxide Microbial Mats

3.2.1. Scanning and transmission electron microscopy

Iron rich microbial mats from Beowulf Spring were observed using cryostage scanning electron microscopy (SEM) and were shown to contain numerous microbial filaments encrusted with Fe-As rich solid phases (Fig. 2). Analysis of these solid phases using EDAX confirmed that the predominant constituents be-

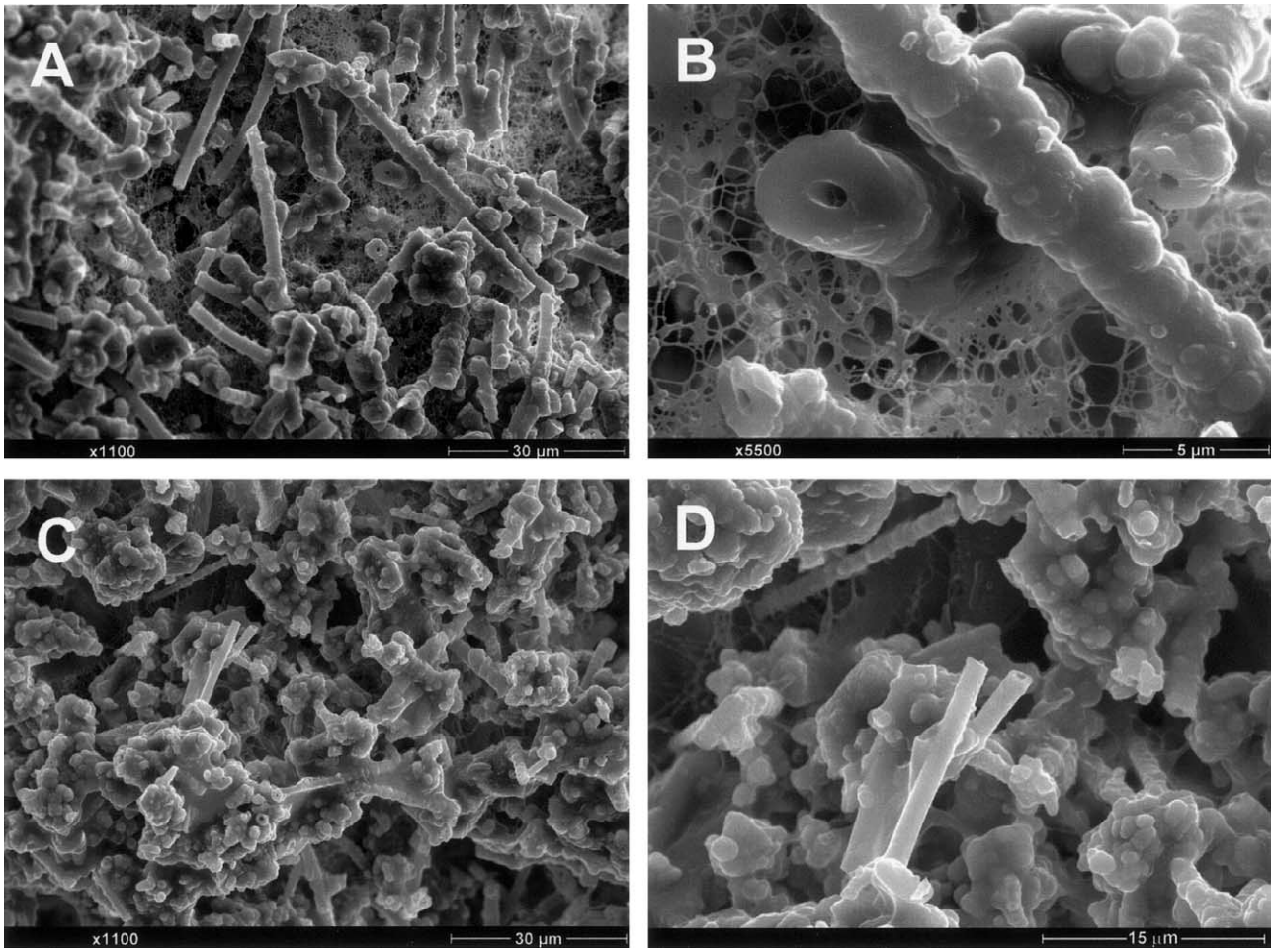

Fig. 2. Scanning electron micrographs (SEM) of Fe mats from Beowulf Spring at site B3 (bottom 2 mm of mat) (A, B) and site B2 (top 2 mm of mat) (C, D). Close-ups of the filamentous As-rich Fe sheaths (molar As: Fe = 0.62 ± 0.01) are shown in B and D, with overall diameters approaching 3 μm. Given the high Fe and As contents of these samples, it was not possible to positively confirm the composition of "web-like" material with fibers as thin as 0.04 μm shown in B.

sides O were As and Fe at As:Fe mole ratios of 0.62 ± 0.01, irregardless of sample location (i.e., across all samples evaluated). Furthermore, the ratios of As:Fe were the same in B2 samples obtained from the top 2 mm or bottom 2 mm of the 2–4 cm thick mats. Total dissolution of solid phase mat samples exhibit consistent molar As:Fe ratios of 0.60 ± 0.01 (Table 3). The ratios observed in Beowulf Spring were similar to As:Fe ratios of 0.7 measured in Fe mats of two additional ASC springs (Langner et al., 2001; Macur, 2004). The encrusted microbial filaments are reminiscent of other Fe(II) oxidizing bacteria, which produce copious amounts of Fe(III) oxyhydroxide as sheaths and precipitates external to the cell wall (Kon-

Table 3. Chemical composition[a] of microbial mats sampled from Beowulf Spring. The composition of mats from site locations B1L, B2 Composite and B3 were essentially identical; consequently, a mean composition is reported here with associated standard errors reported for each element (n = 3).

	Fe	As	TOC[b]	TON[b]	Al	S	K	Na	P	Ca
					%					
Mean	26.02	20.79	1.16	0.14	0.62	0.36	0.090	0.054	0.055	0.007
Std err	0.81	0.61	0.08	0.01	0.10	0.04	0.008	0.003	0.004	0.001
	Ti	Mg	Mn	Ba	Zn	Sb	Cr	Ni	Mo	Cu
					mg/kg					
Mean	217.5	80.0	75.4	64.4	38.7	31.6	24.8	22.6	9.1	3.2
Std err	14.0	6.0	2.3	8.8	1.3	1.6	7.7	3.3	0.7	0.2

[a] All elements except C and N determined using inductively coupled plasma spectrometry (ICP) on HNO_3-$HClO_4$-HF acid digests.
[b] TOC = total organic C, and TON = total organic N; both determined using a LECO furnace.

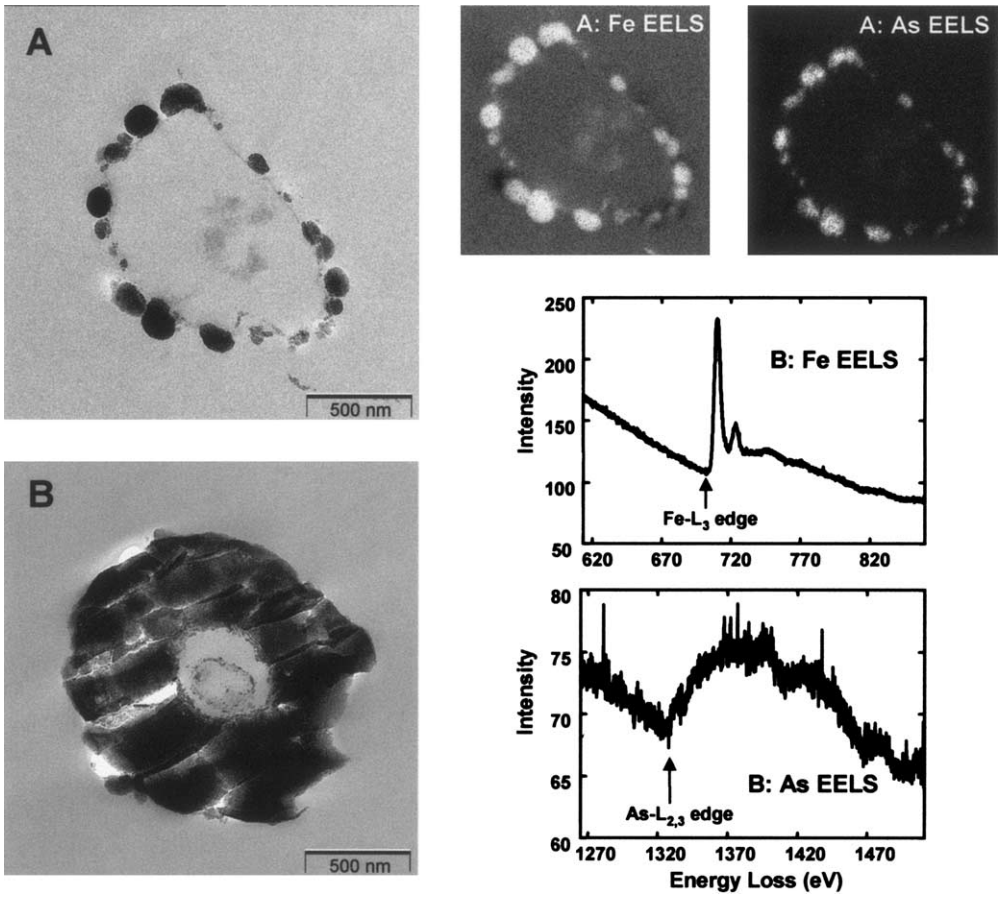

Fig. 3. Transmission electron micrographs (TEM) of unstained cells present in Fe mats of Beowulf Spring from site B2. (A) TEM image of cell surrounded by extracellular, spheroidal solid phase. The larger spheres shown here have diameters ranging from 0.1 to 0.2 um. The corresponding ESI images (A) were generated using a three window power law (15 eV windows) across the Fe and As edges, and confirm the importance of As coprecipitation during the mineralization of HFO. (B) Cross section of an Fe-As encrusted filament showing a 0.45 μm diameter cell surrounded by an Fe-As solid phase sheath with an average thickness of ~0.5 μm. The corresponding PEELS spectra of extracellular solid phase (B) reveal prominent Fe-$L_{2,3}$ and As-$L_{2,3}$ edges.

hauser, 1998). Epoxy impregnated thin sections of the Fe rich mats at site B2 were evaluated using optical microscopy and indicated that the majority of microbial filaments were oriented parallel to the direction of spring flow, yielding a laminar appearance (not shown). In samples evaluated from site B2, irregardless of whether they were from the top or bottom of the mat, microbial filaments were clearly the fundamental units responsible for accumulation and deposition of Fe in these laminar mats.

Subsamples of solid phase mat material from site B2 and B3 were fixed with gluteraldehyde, impregnated with epoxy and thin sections analyzed using TEM/PEELS. Cross sectional images of microbial filaments revealed numerous microorganisms with sheaths exceeding 0.5 μm in thickness (Fig. 3). Scanning electron micrographs show that the total filament diameter including the Fe sheath can approach 3 μm (Figs. 2B,D). Many cells also exhibited small 0.02–0.1 μm diameter spheres as isolated solid phases encircling the outer cell wall (Fig. 3A). The composition of these extracellular solid phases was confirmed using PEELS to be predominantly Fe, As and O and electron spectroscopic images (ESI) confirm the spatial coexistence of these elements (Figs. 3A,B). Selected area electron diffraction experiments were also conducted on many different individual Fe-rich particles, however, no spots or ring patterns characteristic of crystalline phases were observed. In samples from either the top or bottom 2 mm of Fe mat, we observed numerous cross- and semilongitudinal sections of cells exhibiting either (i) isolated spheres of Fe-As rich phases external to the cell wall (as in Fig. 3A), (ii) thick fully encrusted Fe-As sheaths (as in Fig. 3B), or (iii) no obvious Fe nucleation outside the cell wall. This range in the degree of Fe encrustation and sheath morphology may simply be due to different stages of microbial growth and subsequent deposition of As-rich Fe solid phases. Alternatively, these variations represent different microbial populations, which could form Fe solid phases via different mechanisms.

3.2.2. X-ray diffraction

Solid phase samples from Beowulf Spring were also analyzed using standard and synchrotron-based XRD (Fig. 4). The synchrotron XRD spectra (S-XRD) of a composite sample at

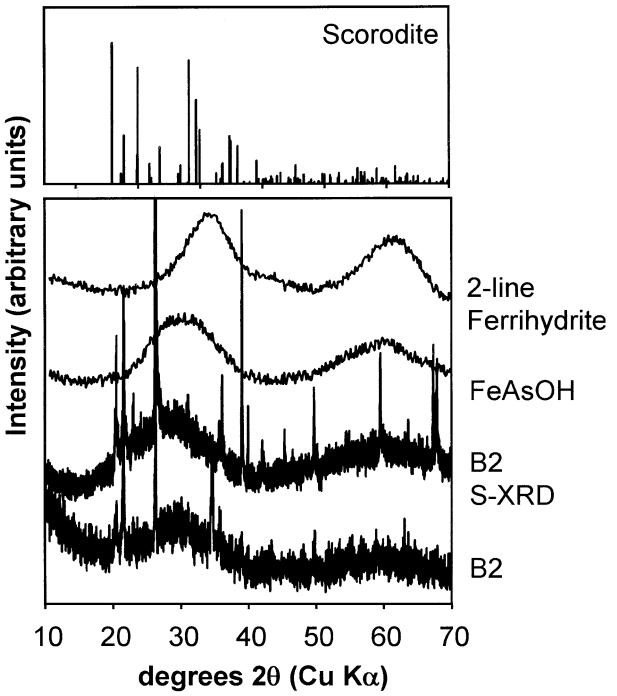

Fig. 4. Representative X-ray diffraction patterns of Beowulf Spring samples from site B2, obtained using both conventional (B2) and synchrotron-based XRD (B2 S-XRD). The patterns are compared with diffraction patterns of arsenate-containing ferrihydrite (FeAsOH), 2-line ferrihydrite, and well crystalline scorodite. The reference patterns are based on published diffraction patterns of scorodite (Hawthorne et al., 1976), and amorphous ferric arsenate and ferrihydrite (Carlson et al., 2002).

site B2 is representative of other solid phase mat samples and contained several sharp diffraction peaks imprinted over a few broad, low intensity Bragg peaks at 29 and 60 °2θ, (2.8 and 1.45 Å). The sharp peaks indicate the presence of a variety of crystalline SiO_2 polymorphs (e.g., tridymite, cristobalite and opaline silica; Smith, 1998), but the spectra show no evidence to suggest the presence of well- crystalline Fe or As phases. In contrast, the broad diffraction maxima are characteristic of other amorphous As-rich HFOs (Pichler et al., 1999; Carlson et al., 2002). The broad features are also similar to those of 2-line ferrihydrite (Drits et al., 1993; Carlson et al., 2002), but definitely inconsistent with reported diffraction patterns of scorodite (crystalline $FeAsO_4 \cdot 2H_2O$). While 2-line ferrihydrite and HFO contain 2 principal diffraction peaks (at ~2.6 and 1.5 Å, 33 and 60 °2θ) near those observed in Beowulf samples, the XRD patterns for Beowulf samples show a characteristic shift in these peaks towards larger *d*-spacings (at ~3.1 and 1.6 Å, 29 and 58 °2θ) observed as a function of As loading in synthetic As(V)-HFOs (Rancourt et al., 2001; Carlson et al., 2002). The XRD data of Beowulf samples suggest that As is likely associated with the Fe phase via adsorption on a ferrihydrite-like phase. It is well established that arsenate is strongly retained through adsorption or coprecipitation with ferrihydrite and other HFOs (e.g., Waychunas et al., 1993; Fendorf et al., 1997), although the structure of the resulting solids is not yet fully resolved.

3.2.3. X-ray absorption spectroscopy (XANES/EXAFS)

Definitive valence state information and estimates of the As-Fe bonding environments in mat solid phases were obtained for sites B1L, B1D and for top and bottom mat locations at sites B2 and B3 using XANES spectroscopy (Fig. 5, Table 4). The As absorption edge for all Beowulf samples was located at 11874 eV, similar to that obtained for arsenate [As(V)] standards (Fig. 5). In contrast, arsenite has an absorption edge at 11871 eV (Fig. 5), and other reduced As solid phases (As_2S_3, AsS, and FeAsS) all have absorption edges at lower energy. Consequently, the predominant valence state of As in these solid phases was As(V). Moreover, linear combination fitting of XANES spectra from the Beowulf samples suggested that there was no detectable As(III) in these solid phases. Iron XANES spectroscopy was also performed to determine the fraction of Fe(II) in the samples, and in each case, all detectable Fe was determined to be Fe(III) (Table 5).

Results from X-ray diffraction of solid phases from Beowulf Spring (Fig. 4) suggest that As is present as a coprecipitate or adsorbed phase with a ferrihydrite-like HFO, rather than a discrete Fe(III)-arsenate mineral. Results of fitting As EXAFS spectra confirm that for all Beowulf samples analyzed, arsenate is retained through adsorption on HFO (Fig. 6). The local As structure is dominated by an As-O shell (CN = ~4) at a distance of 1.68 Å, typical of tetrahedral coordination in arsenate. More distant shells have increased complexity, containing two As-Fe shells at nominal distances of 2.82 and 3.33 Å (Table 4). These distances are indicative of edge-sharing and

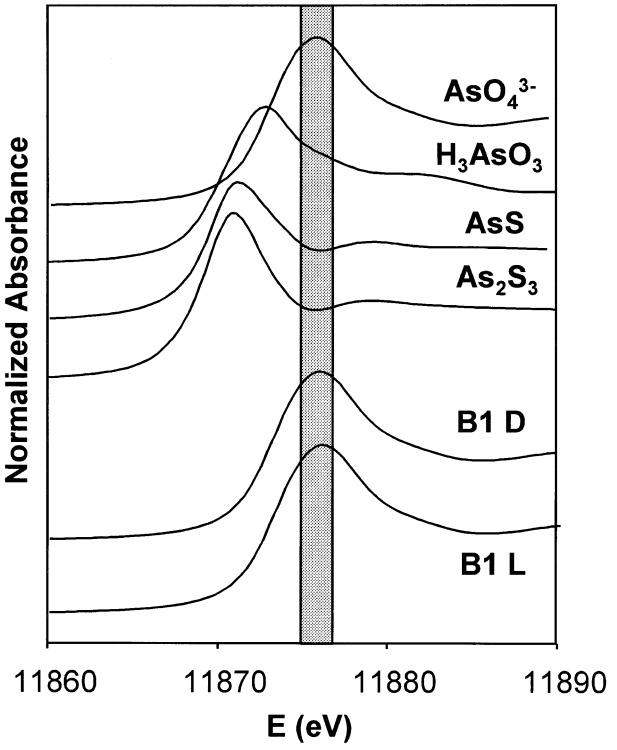

Fig. 5. Arsenic XANES of representative As-rich Fe oxyhydroxide solid phases sampled from Beowulf Spring. The absorption edge of all Beowulf samples was near 11874 eV, indicative of arsenate [As(V)].

Table 4. Arsenic local structure of As-rich Fe oxyhydroxides isolated from Beowulf Spring as determined by fitting EXAFS data. For each sample, XANES data showed that all As was present was As(V). The coordination number (CN) is typically accurate to within ±1, interatomic distance (R) within ± 0.02 Å; σ^2 represents the variance in R. For all of the media, E_0 was set at ≈ 11874 eV, typical of As(V).

Sample	Shell	CN	R (Å)	σ^2 (Å^2)
B1 Light	As-O	4[c]	1.68	0.0026
	As-Fe_1[a]	0.97	2.82	0.01[c]
	As-Fe_2[b]	1.81	3.33	0.01[c]
B1 Dark	As-O	4[c]	1.68	0.0023
	As-Fe_1[a]	0.96	2.83	0.01[c]
	As-Fe_2[b]	2.27	3.32	0.01[c]
B2 Bottom	As-O	4[c]	1.68	0.0018
	As-Fe_1[a]	1.07	2.83	0.01[c]
	As-Fe_2[b]	2.49	3.33	0.01[c]
B2 Top	As-O	4[c]	1.69	0.0017
	As-Fe_1[a]	1.21	2.83	0.01[c]
	As-Fe_2[b]	1.97	3.32	0.01[c]
B3 Bottom	As-O	4[c]	1.69	0.0031
	As-Fe_1[a]	1.09	2.85	0.01[c]
	As-Fe_2[b]	1.98	3.33	0.01[c]
B3 Top	As-O	4[c]	1.69	0.0024
	As-Fe_1[a]	0.91	2.86	0.01[c]
	As-Fe_2[b]	1.95	3.33	0.01[c]
As-Fe mixed precipitate (0.7 As:Fe)[d] (Manceau, 1995)	As-O	4[c]	1.68	0.0025
	As-Fe_1[a]	0.6	2.83	~0.012[c]
	As-Fe_2[b]	2.3	3.26	~0.012[c]
Scorodite (Waychunas et al., 1993)	As-O	4[c]	1.68	0.0012
	As-Fe	4[c]	3.36	0.0052

[a] Defined as the bidentate, mononuclear bridging complex.
[b] Defined as the bidentate, binuclear bridging complex.
[c] Fixed during fitting.
[d] The fit parameters for the As-O shell and σ^2 for the As-Fe shells are not included explicitly in Manceau (1995). Consequently, the fit parameters for the As-O shell are based on spectral fitting by Waychunas et al. (1993) of the same data. The σ^2 for the As-Fe shells was fixed at a σ^2 that was 0.03 Å greater than a reference sample of lepidocrosite (γ-FeOOH), and the values reported here are approximations of that σ^2 based on our fits of lepidocrosite data.

corner-sharing coordination to Fe(III) octahedra, and distinct from scorodite. There are no obvious trends in the coordination number or disorder in the As-Fe shells across different sampling sites in Beowulf Spring, suggesting that both types of As surface complexes are present in all samples. The EXAFS spectra are similar to those observed for As(V) adsorbed on ferrihydrite, or coprecipitated with Fe(III) oxyhydroxides (e.g., Waychunas et al., 1993, 1995). The As(V) associated with these HFOs is strongly bound as both a bidentate binuclear and a bidentate mononuclear complex. The formation of As(V)-HFOs in ASC springs may be important in moderating the concentration of toxic As(V) over longer time scales. Furthermore, these amorphous solid phases may ripen with aging and eventually result in the incorporation of As(V) within more crystalline minerals (Ford et al., 2002).

Iron K-edge EXAFS was useful to further examine the structure of As(V)-HFOs found in Beowulf Spring. Iron EXAFS spectra show only one strong feature, attributed to a disordered Fe-O shell with an interatomic distance near 2.0 Å (Fig. 7, Table 5). A weak Fe-As shell was also observed, which is similar to and consistent with that determined using As EXAFS (Table 4). Furthermore, the low Fe-As coordination number determined using Fe EXAFS is consistent with the

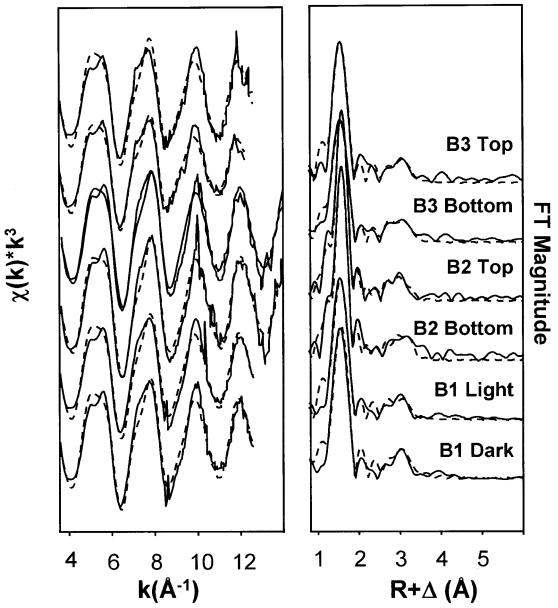

Fig. 6. Arsenic K-edge EXAFS spectra of As-rich Fe oxyhydroxides from Beowulf Spring. Both the k-weighted χ(k) functions (A) and their Fourier-transforms (B) are plotted. The solid lines are the experimental data, and the dotted lines are fits.

Table 5. Iron local structure of solid phase mat samples from Beowulf Spring. For each sample, XANES data showed that all Fe was present was Fe(III). The Fe-Fe shells are included for comparison; however, none were statistically justified or included in final fits. The coordination number (CN) is typically accurate to within ±1, interatomic distance (R) within ± 0.02 Å; σ^2 represents the variance in R. For all of the media, E_0 was about 7120 eV, typical of Fe(III).

Sample	Shell	CN	R (Å)	σ^2 (Å^2)
B1 Light	Fe-O	6[c]	1.99	0.011
	Fe-Fe_1[a]	0.19	3.03	0.01[d]
	Fe-As[b]	0.76	3.31[d]	0.01[d]
	Fe-Fe_2[c]	0.24	3.63	0.01[d]
B1 Dark	Fe-O	6[c]	1.98	0.0097
	Fe-Fe_1[a]	0.18	2.91	0.01[d]
	Fe-As[b]	1.11	3.32[d]	0.01[d]
	Fe-Fe_2[c]	0.55	3.63	0.01[d]
2-line Ferrihydrite	Fe-O	3.12	1.94	0.0084
(Waychunas et al., 1993)	Fe-O	2.13	2.09	0.0084
	Fe-Fe_1[a]	1.53	3.03	0.005
	Fe-Fe_2[c]	2.06	3.45	0.005
6-line Ferrihydrite	Fe-O	3	1.96	n/d
(Drits et al., 1993; Manceau	Fe-O	3	2.21	n/d
and Drits, 1993)	Fe-Fe_1[a]	3.0	3.01	~0.013
	Fe-Fe_2[c]	6.5	3.44	~0.013
As-Fe mixed precipitate (0.7 As:	Fe-O	3.85	1.96	0.0084
Fe) (Waychunas et al., 1993)	Fe-O	2.46	2.10	0.0084
	Fe-Fe_1[a]	0.83	3.04	0.01[d]
	Fe-As[b]	0.79	3.23	0.0097

[a] Defined as edge-sharing Fe octahedra. The distances are constrained based on those found for 2-line ferrihydrite (Manceau and Drits, 1993).
[b] The Fe-As shell represents the bidentate, binuclear complex. To minimize the number of variables, the interatomic distance and Debye-Waller factor are constrained to those determined by As K-edge EXAFS. The other Fe-As shell is not included in fitting because it is occluded by the Fe-Fe shells.
[c] Defined as corner-sharing Fe octahedra.
[d] Fixed during fitting.

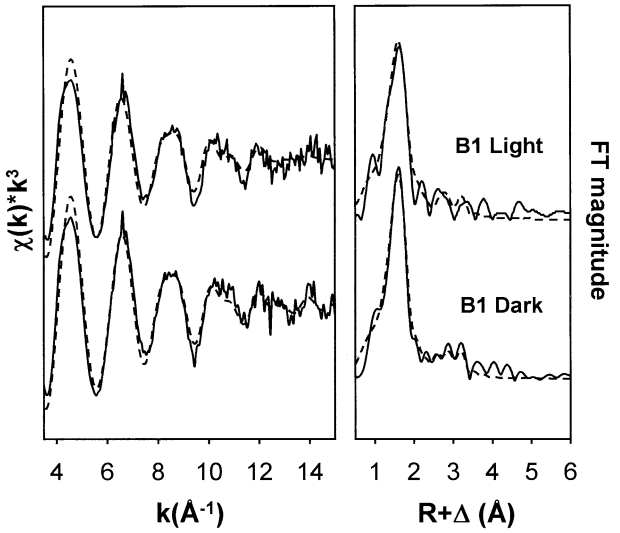

Fig. 7. Iron K-edge EXAFS of As-rich Fe oxyhydroxides from Beowulf Spring. Both the k-weighted χ(k) functions (A) and their Fourier-transforms (uncorrected for phase shift) (B) are plotted. The solid lines are the experimental data, and the dotted lines are fits.

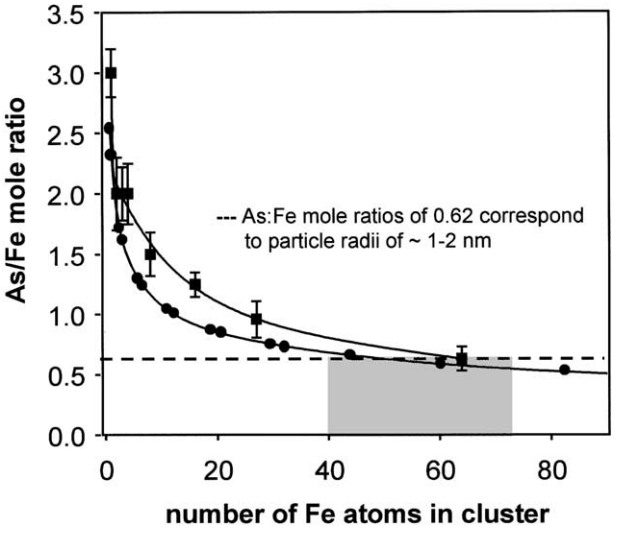

Fig. 8. Number of Fe atoms in a cluster versus As:Fe ratio assuming complete site saturation with arsenate. The square symbols indicate site saturation based on crystallographic limitations (the number of bridging hydroxyls present on the surface), where the error associated with these values is based on possible variation in crystal morphology. The circle symbols assume spherical particles and an adsorption density of 3.5 sites/nm^2, similar to that reported by Dzombak and Morel (1990).

formation of arsenate surface complexes on ferrihydrite, and suggests that only a portion of Fe atoms are coordinated directly to arsenate. However, there is little evidence for the presence of Fe-Fe interactions (Fig. 7, Table 5) that typify ordered Fe hydroxide phases (Combes et al., 1989; Manceau and Drits, 1993). In fact, Fe-Fe shells were not justified in fitting the Fe EXAFS spectra of Beowulf samples, and their coordination numbers are exceedingly low when fixed to ferrihydrite-like coordination (Table 5). The lack of Fe-Fe coordination indicates that any HFO formed is highly disordered, in part due to the high concentrations of As which are complexed to the edges and corners of Fe(III) octahedra. The diffraction data and the EXAFS data are consistent with the observation that 100% of the Fe and As present in these solid phases was extractable with NH_4-oxalate (pH = 3), an extraction method that correlates with the 'amorphous Fe oxide' fraction (Loeppert and Inskeep, 1996).

The particle size of the As(V)-HFOs from Beowulf Spring can be estimated by examining the quantity of arsenate that can theoretically be adsorbed to −FeOH surfaces as a function of the number of Fe atoms in a HFO particle. For samples from Beowulf Spring, the particle diameter would have to be between 1 and 2 nm to have sufficient surface sites to accommodate As:Fe mole ratios of ~ 0.62 (Fig. 8). The presence of amorphous or nanocrystalline phases is consistent with the high degree of disorder observed by diffraction and EXAFS. However, the low N_2-BET surface areas (5 m^2/g) and TEM images of these samples suggest that apparent particle diameters range from 0.1 to 0.5 μm, much larger than predicted based on arsenate adsorption densities. Aggregation and or consolidation of As(V)-HFO nanophases is likely responsible for the low measured surface areas observed in these samples. Rancourt et al. (2001) proposed similar aggregation processes during the formation of disordered HFOs in hydrothermal vents.

3.3. Microbial Community Analysis Based on 16S rDNA Sequence Data

As demonstrated in SEM and TEM micrographs (Figs. 2–3), the Fe-As rich mats contain numerous microorganisms, many of which show various stages of Fe encrustation. The microbial populations present in these mats were evaluated using DNA extraction, PCR amplification of 16S rDNA, separation of 16S fragments using DGGE, and subsequent sequence analysis of purified DGGE bands. Community profiles for sites B1L, B1D, B2 top and bottom, and a composite (whole sample) of B2 were obtained using both universal archaeal and bacterial primers (Fig. 9). The majority of DGGE bands from each site were sequenced and compared to sequences deposited in GenBank (based on BLAST searches in May 2003). There were, however, several DGGE bands which could not be purified and sequenced. For reporting purposes, the band numbers and corresponding 16S rDNA sequences obtained from these samples will be referred to as GenBank closest neighbor–like populations. Furthermore, it is understood that band intensity is not always a trustworthy indicator of the numerical abundance of active organisms, due to potential template bias during amplification. However, cultivation-independent approaches avoid the well-established bias inherent in most isolation strategies, and provide a first line of evidence regarding the potential importance of specific microbial populations in a sample. In many cases, the two different primer sets (archaeal and bacterial) resulted in amplification of identical sequences, supporting the identification of potentially dominant microbial populations (Fig. 9). Replicate community profiles were obtained for each site location and the banding patterns were highly reproducible (nearly band for band); consequently, the differences in banding patterns among site locations suggests a distribution of

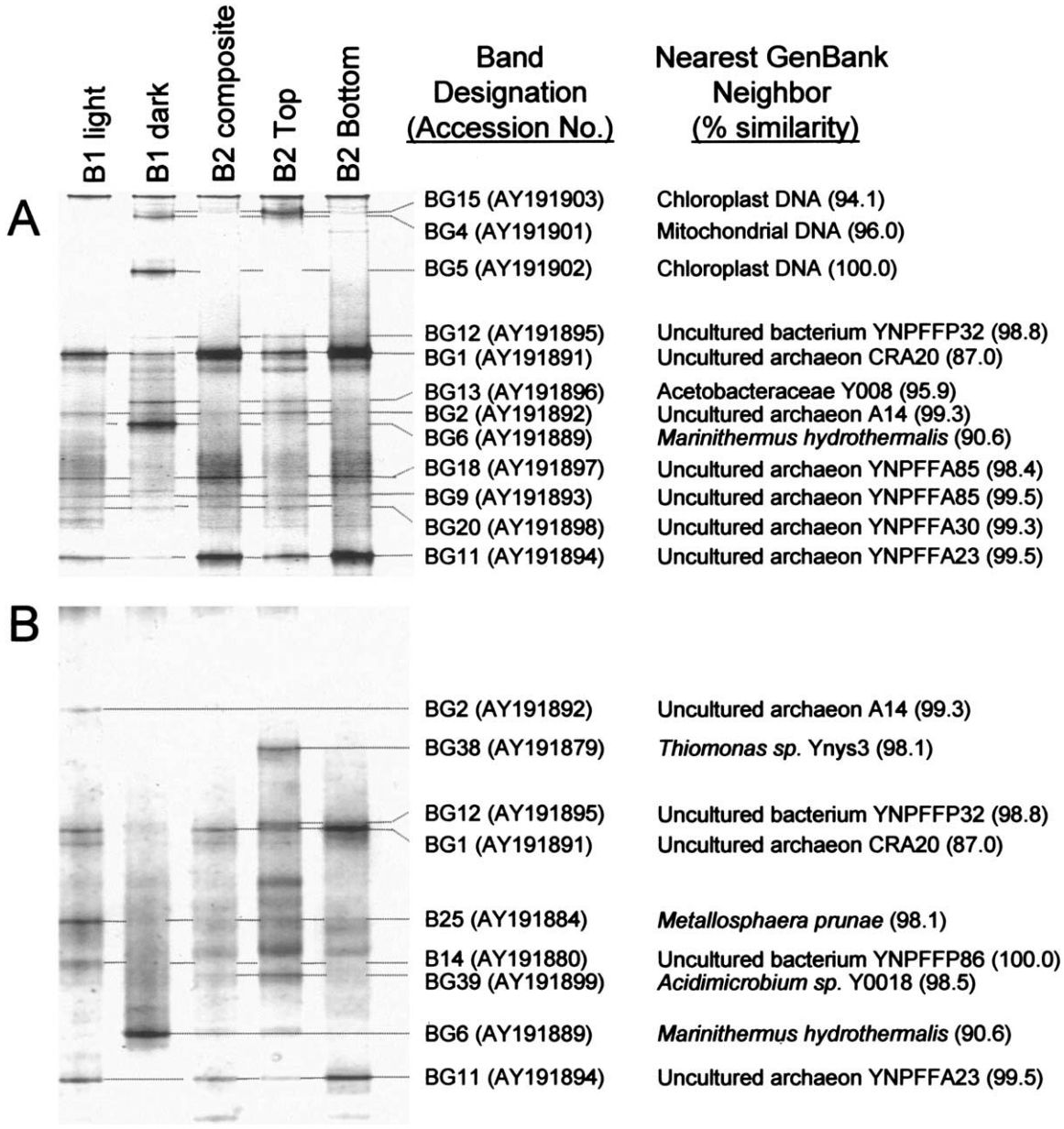

Fig. 9. Microbial community 16S rDNA fingerprints generated using denaturing gradient gel electrophoresis (40–70% gradient) of partial 16S rRNA genes amplified from Beowulf Spring using universal archaeal (A) and bacterial (B) primer sets. Bands that were successfully purified and sequenced are labeled with band designation, corresponding GenBank accession number, nearest GenBank neighbor, and % similarity of band sequence to nearest neighbor sequence. Dotted lines indicate comigrating bands.

different microbial populations across temperature and chemical gradients. Also, samples treated with NH_4-oxalate to remove the Fe sheaths resulted in identical banding patterns to those reported here; consequently, the presence of Fe sheaths did not inhibit effective DNA extraction.

Two intense bands (BG1, BG11) were present in all samples except site B1D (Fig. 9). In both cases, the nearest GenBank neighbors of these 16S sequences were uncultured archaeon clones; BG1 was 87% similar to an uncultured archaeon CRA20 [GenBank Accession no. AF119130] and BG11 was 99% similar to an uncultured archaeon YNPFFA23 [AF391991]. Very little is known about these uncultured archaea except that CRA20 and its close relative in GenBank (clone pEPR113 [AF526987]) originate from samples of deep-sea sediments or hydrothermal vents (Vetriani et al., 1999). Given that the sequence corresponding to BG1 was only 87% similar to CRA20, the archaeon represented by this band is likely a novel organism. Although the sequence corresponding to band BG11 was 99% similar to YNPFFA23 and several other archaeal clones identified at Fairy Falls, YNP (AF391989, AF391990, AF391993), the nearest cultured relative was *Aeropyrum pernix* (AB078015) at

only 89% similarity. Consequently, the organism represented by band BG11 is also a novel uncharacterized archaeon.

Site B1 Dark is located at the terminus of the west source, is considerably cooler (53°C) and exhibits thinner, darker brown (2.5YR 4/4) Fe mats. The dominant band at site B1D for both the archaeal and bacterial primers was BG6 with a partial 16S sequence that was 90% similar to a *Marinithermus hydrothermalis* (AB079382) isolate cultivated from a deep sea vent (Sako et al., 2003). The low 16S similarity suggests that the organism represented by BG6 is also novel and uncharacterized. Interestingly, this *Marinithermus*-like population was only detected at site B1D.

At site B1 Light (64°C), dominant DGGE bands included BG1 and BG11 (described above) and B25, whose corresponding sequence exhibited closest GenBank matches to known S and or Fe oxidizers *Metallosphaera prunae* (X90482, 98% similar) and *M. sedula* (D26491, 97% similar). Site B1L is located in the hotter zone of early Fe deposition ~1 m down gradient from the commencement of Fe mat formation. The Fe mats at this location are thicker and lighter (5YR 5/8) than mats at B1D (2.5YR 4/4). The presence of a *Metallosphaera*-like population at only site B1L is consistent with our observations in a nearby thermal spring where *Metallosphaera*-like populations appear confined to hotter zones (~65°C) of Fe deposition (Macur, 2004).

Moving down gradient to site B2 (59°C), bands BG1 and BG11 (described above) are still important; however, several bands unique to the top 2 mm of site B2 (B2T) are noteworthy. Bands BG38, BG39 and B12 were observed only in sample B2T and correspond to sequences which were most similar (GenBank) to a *Thiomonas* isolate (AF387303, 98% similar), an *Acidimicrobium* sp. isolate Y0018 (AY140240, 98% similar) and an uncultured bacterial clone YNPFFP32 (AF391976, 98% similar), respectively. The 16S sequence of BG38 is 100% identical (in the region analyzed) to a *Thiomonas*-like population observed in 60°C Fe mats in a nearby ASC spring (Macur, 2004), and is closely related to other *Thiomonas* sp. that have been implicated in Fe(II) and or As(III) oxidation in aerobic acid mine drainage environments (Dennison et al., 2001; Morin et al., 2003). Other closest neighbors to the 16S sequence corresponding to BG39 include a thermophilic Fe-oxidizing bacterium TH3 (M79434, Lane et al., 1992; 97% similar), an uncultured bacterial clone (BA46) from extreme acid mine drainage environments at Iron Mountain (AF225450, Bond et al., 2000; 97% similar), an Fe-oxidizing *Ferromicrobium acidophilum* isolate (AF251436, 97% similar) and an *Acidimicrobium ferroxidans* isolate (U75647, Clark and Norris, 1996; 96% similar). These closest neighbors all share characteristics of either being acidophilic and thermophilic, or acidophilic, and most have been shown to be associated with Fe(II) oxidation. Finally, the 16S sequence corresponding to BG12 is closely related to other uncultured bacteria from YNP, including clones obtained from Fairy Falls, YNP (YNPFFP32) (AF391976, 98% similar) and Ragged Hills in Norris Basin, YNP (YNPRH54A, 95% similar). The later sequence represents an uncultured planctomycete, organisms which are known for surface attachment via stalks in aquatic systems. However, given the lack of cultured relatives to BG12 and the likelihood that this sequence also represents a novel organism, it is difficult to infer possible function of this population in the Fe mats of Beowulf Spring.

Sequences of DGGE bands of intermediate and low intensity were also characterized and compared to 16S sequence data in GenBank, and these bands are also represented by a large number of uncharacterized organisms. Bands BG2 and B14 were fairly intense at site B1 Light, while BG2 was a minor band at sites B1 Dark and B2 Top. Band BG2 corresponds to a 16S sequence which exhibited a 99% match to an uncultured archaeon clone A14 (AF325186) observed in Fe mats of a similar ASC spring (Jackson et al., 2001). The next closest neighbor to BG2 at 94% similarity was a clone pUWA2 (AB007307) obtained from geothermal environments in Japan (Takai et al., 1999); consequently, BG2 also represents a novel population with no closely related cultured organisms. Band B14 corresponds to a 16S sequence which was 100% identical to an uncultured bacterial clone (YNPFFP86) from Fairy Falls (AF391980) and a clone (AF356015) from acidic hydrothermal waters of volcanic environments in New Zealand (Donachie et al., 2002). Furthermore, B14 was also identified as one of two sequences present in enrichment isolation cultures from an ASC thermal spring that were actively oxidizing Fe(II) (B. Kocar, unpublished data). Finally, less intense bands including BG9, BG13, BG18 and BG20 were present in many of the Fe mat samples from Beowulf Spring. The sequences corresponding to bands BG9, BG18 and BG20 were closely related to other uncultured archaea obtained from Fairy Falls, YNP. For example, bands BG9 and BG18 represent very similar sequences (99% similar to one another) that were 98% similar to an uncultured archaeon clone YNPFFA85 (AF391992) and 95% similar to uncultured clones YNPFFA1, YNPFFA4 and YNPFFA23 (AF391989-91). These bands also appear to have no closely related cultured organisms, so they too represent novel archaeal populations for which there is little physiologic information. Band BG20 corresponds to a 16S sequence which is 99% similar to uncultured archaeal clones YNPFFA30 (AF391995) and YNPFFA52 (AF391996). The closest cultivated neighbor to BG20 at 93% similarity was the isolate *Acidianus ambivalens*, newly classified from what was *Desulfurolobus ambivalens* (Fuchs et al., 1996). Band BG13 is contributed by a population that is only 95% similar to a heterotrophic acidophilic bacterium isolated from YNP (AY140238), and only 93% similar to *Gluconacetobacter sacchari* (AF127409), an acetic acid bacterium (Franke et al., 1999).

In summary, the 16S rDNA sequences obtained from the Fe mats of Beowulf Spring indicate the presence of diverse and often novel archaea and bacteria. Although several sequences detected in these Fe mats were closely related to 16S sequences of cultured organisms with known capabilities to oxidize Fe(II) and or As(III), the majority of sequences obtained from the mats were not closely related to cultured organisms. Consequently, very little is known regarding the potential metabolic or physiologic attributes of the organisms represented by these sequences, and in most cases, their role in the deposition of As(V)-rich Fe(III) oxyhydroxide mats cannot be estimated using phylogenetic inference.

3.4. Mechanisms of As(V)-HFO Biomineralization

We have presented a comprehensive characterization of As(V)-HFO solid phases associated with microbial mats in a high As, acid thermal spring in Norris Geyser Basin, YNP. The

subject spring is representative of at least one major type of acid-sulfate-chloride (ASC) geothermal spring distributed across different geographical locations within YNP. The poorly ordered HFO phases that form in microbial mats of the 53–65°C temperature zones of Beowulf Spring exhibit mole ratios of As:Fe of 0.62, similar to other high-As HFOs observed in acid-mine drainage environments and other ASC springs of YNP. Furthermore, the data presented in the current study show definitively that the As present in these phases is As(V), and that molecular As-Fe distances are consistent with edge-sharing and corner-sharing coordination of arsenate with Fe(III) octahedra as bidentate binuclear and bidentate mononuclear complexes, similar to observations made on synthetic As-rich ferrihydrites or coprecipitated As(V)-HFO phases (Waychunas et al., 1993; Rancourt et al., 2001; Carlson et al., 2002). The lack of a significant Fe-Fe shell obtained using Fe edge EXAFS suggests a highly disordered Fe(III)-hydroxide phase, consistent with XRD patterns and the inability to obtain electron diffraction. Theoretical particle size estimates based on knowledge of the As:Fe mole ratio and the nature of surface complexation from As EXAFS suggest that these nanocrystalline phases are approximately 1–2 nm in diameter, but that they aggregate into larger particles during formation external to the cell wall.

The coprecipitation of As(V) with the Fe(III) oxyhydroxide phase appears to commence during the nucleation of Fe clusters external to cell membranes (Fig. 3A). The aqueous phase As species present in the Fe depositional zone include both $H_3AsO_3^o$ and $H_3AsO_4^o/H_2AsO_4^-$. Consequently, formation of Fe(III)-OH clusters occurs in the presence of approximately equal concentrations of 12 μM As(III) and As(V). It is noteworthy that the resulting solid phases associated with microbial cell walls contain predominantly As(V), when it is well established that $H_3AsO_3^o$ [As(III)] also adsorbs strongly to HFOs via a similar bidentate surface complex (Manning et al., 1998). However, the pH dependence of arsenate versus arsenite sorption (Manning et al., 1998; Sun and Doner, 1998) suggests that As(V) surface complexation would be favored at native spring pH values of 3.1. Alternatively, additional oxidation of As(III) may be mediated by the same microorganisms responsible for Fe(II) oxidation or other community members in close proximity. The likelihood that As(III) sorbs to the HFO phases and is then later oxidized to As(V) via abiotic oxidation by Fe(III) is low based on reports of the stability of As(III) on Fe oxide surfaces (Manning et al., 1998) and the fact that As(III) oxidation has been shown to require the presence of live mat (Langner et al., 2001). It is also important to note that the HFO phases formed in Beowulf Spring contain very little S and essentially no boron (B), despite the high concentrations of B (0.8 mM) and sulfate (1.3 mM) in the geothermal source waters flowing over these mats. The pH dependent sorption of these oxyanions is such that arsenate sorption is strongly favored at pH 3.

3.5. Microbial Controls on Geochemical Processes

Biomineralization processes are of considerable interest in geobiology, industrial corrosion, and biomedical sciences, and can represent important contributions to the biogeochemical cycle for many elements, often yielding clues regarding evidence of past microbial life preserved in geologic strata. The mechanism of formation of As(V)-HFO solid phases in this microbial mat is clearly linked to microbial processes, either through oxidation of Fe(II) as an electron donor for chemolithotrophic metabolism and or as a result of biomass-induced oxidation and subsequent nucleation of the Fe phase on the cell walls of microorganisms (Figs. 2–3). These suggestions represent testable hypotheses, that with further experimentation, will ultimately define a functional role for specific members of the microbial community. It is through our understanding of natural systems that we begin to appreciate the geomicrobial complexity characteristic of other contaminated environments, and the difficulty of implementing remediation strategies that ultimately depend on microbial activity, and more specifically on the microbial activity of specific populations! Further work in this geothermal model system will focus on establishing definitive linkages among phylogenetically defined populations and specific geochemical processes (e.g., As(III) oxidation, Fe(II) oxidation, Fe(III) reduction, CO_2 fixation). We speculate that the microbial populations detected in these mats using molecular methods are uniquely adapted to these environments, and in turn have coevolved with other organisms of the community yielding diverse metabolisms reflective of specific geochemical parameters and or processes. In this regard, detailed characterization of model microbial communities provides an excellent opportunity for assessing how microbial speciation is linked to geochemical speciation and the ecological factors that control microbial population dynamics.

Analysis of 16S rDNA sequences present in As(V)-HFO mats of Beowulf Spring suggest that several uncultured archaea and bacteria are important microbial populations in this community, as well as organisms that have closest neighbors known to be associated with either Fe(II) or As(III) oxidation. TEM images of these microbial cells suggest the possibility that different degrees and morphologies of Fe encrustation may reflect contributions from different microorganisms. Molecular data on the distribution of 16S rDNA sequences in the Fe-rich mats are consistent with this hypothesis and suggest that several different microbial populations may be important in the formation of As(V)-HFO mats. One of the central tenants of microbial diversity and biologic speciation in natural systems relates to the importance of habitat and geochemical attributes in potentially defining the evolution of microbial species, where unique microbial species are distributed across gradients of temperature and or aqueous chemistry (Ward, 1998). Indeed, the 16S sequence data obtained in the present study supports the hypothesis that the distribution of microbial populations varies across physical and chemical gradients because of adaptations to specific microenvironments. Even these reasonably simple model communities are defined by several different microbial populations, providing opportunities for understanding networks among physiologically distinct groups of microorganisms. However, the actual function of microorganisms represented by the 16S sequences identified in these mats is difficult to ascertain, and especially considering that many sequences have no closely related cultured organisms. This suggests that other complimentary techniques will be necessary to truly couple microbial population analysis with geochemical processes, such as application of functional genomics or culti-

vation and subsequent physiologic characterization of novel organisms (Reysenbach and Shock, 2002).

Despite these limitations and opportunities for future progress, several sequences represented by *Metallosphaera*-like, *Thiomonas*-like and *Acidimicrobium*-like populations were found within the Fe mats and are closely related to isolates that have been shown to oxidize Fe(II) and or As(III). For these sequences, we can infer that the corresponding microbial populations present in the mat samples likely play a role in the oxidation of Fe(II) to form As(V)-HFO. Differences in microbial community structure across mat locations (e.g., B1D versus B1L) again suggest that microbial speciation may occur over short distances in these environments, responding to changes in aqueous and solid phase chemistry and or temperature. One of the challenges for future research in geomicrobiology is to utilize the descriptive information (such as that presented in this study) necessary for defining natural environments more systematically to establish consistent patterns of sequence distribution in relation to geochemical properties and processes. These observations will assist in defining the networks controlling chemical and biologic energy flow in natural microbial communities. It has been suggested that model microbial communities provide opportunities for understanding links between genomics and biogeochemical networks in environmental contexts that are well defined, not overly complicated in numbers of different species, yet that exhibit phylogenetic and metabolic diversity (Newman and Banfield, 2002). In this regard, further ecological and genomic studies focused on microbial-mineral interactions in extreme geothermal environments will contribute to discovery of novel microorganisms whose metabolisms are understood in the context of biogeochemical function. Simultaneously, these efforts will contribute to our understanding of the geochemical factors responsible for the evolution of microbial species.

Acknowledgments—This work was supported by funding from the National Aeronautics and Space Administration (NAG5-8807) via the Thermal Biology Institute at Montana State University and the Montana Agricultural Experiment Station (911398). X-ray absorption and diffraction data were collected at the Stanford Synchrotron Radiation Laboratory (SSRL), a facility operated by the Department of Energy Office of Basic Energy Science. The authors appreciate input from H. W. Langner and D. K. Nordstrom regarding field sampling and analytical protocols, and S. Brumfield for assistance obtaining TEM and EELS images. Finally, the authors appreciate support from C. Hendrix and J. Varley, Yellowstone Center for Resources, Yellowstone National Park, WY for permitting this work.

Associate editor: L. B. Benning

REFERENCES

Allison J. D., Brown D. S., and Novo-Gradac K. J. (1991) *MINTEQA2/PRODEFA2, a Geochemical Assessment Model for Environmental Systems: Version 3.0 User's Manual*. Environmental Research Laboratory, Office of Research and Development, USEPA, Athens, Georgia.

Altschul S. F., Madden T. L., Schäffer A. A., Zhang J., Zhang Z., Miller W., and Lipman D. J. (1997) Gapped BLAST and PSI-BLAST: A new generation of protein database search programs. *Nucleic Acids Res.* **2,** 53389–3402.

American Public Health Association (APHA). (1998a) Part 4500: NH_3 H. In *Standard Methods for the Examination of Water and Wastewater* (eds. L. S. Clesceri, A. E. Greenberg, and A. D. Eaton) pp. 4-111–4-112. APHA.

American Public Health Association (APHA). (1998b) Part 4500: S^{2-} D. In *Standard Methods for the Examination of Water and Wastewater* (eds. L. S. Clesceri, A. E. Greenberg, and A. D. Eaton) pp. 4-165–4-166. APHA.

Anderson G. L., Williams J., and Hille R. (1992) The purification and characterization of arsenite oxidase from *Alcaligenes faecalis*, a molybdenum-containing hydroxylase. *J. Biol. Chem.* **267,** 23674–23682.

Ball J. W., McCleskey R. B., Nordstrom D. K., Holloway J. M. and Verplanck P. L. (2002) Water-chemistry data for selected springs, geysers and streams in Yellowstone National Park, Wyoming 1999–2000. Open-File Report 02-382. USGS.

Bond P. L., Smriga S. P., and Banfield J. F. (2000) Phylogeny of microorganisms populating a thick, subaerial, predominantly lithotrophic biofilm at an extreme acid mine drainage site. *Appl. Environ. Microbiol.* **6,** 63842–3849.

Carlson L., Bigham J. M., Schwertmann U., Kyek A., and Wagner F. (2002) Scavenging of As from acid mine drainage by schwertmannite and ferrihydrite: A comparison with synthetic analogues. *Environ. Sci. Technol.* **36,** 1712–1719.

Clark D. A. and Norris P. R. (1996) *Acidomicrobium ferrooxidans* gen. nov., sp. nov: Mixed-culture ferrous iron oxidation with *Sulfobacillus* species. *Microbiology* **142,** 785–790.

Clarke W. A., Konhauser K. O., Thomas J. C., and Bottrell S. H. (1997) Ferric hydroxide and ferric hydroxysulfate precipitation by bacteria in an acid mine drainage lagoon. *FEMS Microbiol. Rev.* **20,** 351–361.

Combes J. M., Manceau A., Calas G., and Bottero J. Y. (1989) Formation of ferric oxides from aqueous solutions: A polyhedral approach by x-ray absorption spectroscopy: I. Hydrolysis and formation of ferric gels. *Geochim. Cosmochim. Acta* **53,** 583–594.

Cummings D. E., Caccavo F., Jr., Fendorf S. E., and Rosenzweig R. F. (1999) Arsenic mobilization by the dissimilatory Fe(III)-reducing bacterium *Shewanella alga* BrY. *Environ. Sci. Technol.* **33,** 723–729.

Dennison F., Sen A. M., Hallberg K. B., and Johnson D. B. (2001) Biological versus abiotic oxidation of iron in acid mine drainage waters: An important role for moderately acidophilic, iron-oxidising bacteria. In *Biohydrometallurgy: Fundamentals, Technology, and Sustainable Development* **11a** (eds. V. T. Ciminelli and O. Garcia, Jr.), pp. 493–501. Elsevier.

Donachie S. P., Christenson B. W., Kunkel D. D., Malahoff A., and Alam M. (2002) Microbial community in acidic hydrothermal waters of volcanically active White Island, New Zealand. *Extremophiles* **6,** 419–425.

Donahoe-Christiansen J., D'Imperio S., Jackson C. R., Inskeep W. P., and McDermott T. R. (2004) An arsenite-oxidizing *Hydrogenobaculum* isolated from an acid-sulfate-chloride thermal spring in YNP, USA. *Appl. Environ. Microbiol.* **70,** 1865–1868.

Drits V. A., Sakharov B. A., Salyn A. L., and Manceau A. (1993) Structural model for ferrihydrite. *Clay Min.* **28,** 185–207.

Dzombak D. A. and Morel F. M. M. (1990) *Surface Complexation Modeling: Hydrous Ferric Oxide*. Wiley.

Ehrlich H. L. (1990) *Geomicrobiology* 2nd ed. Marcel Dekker.

Fendorf S., Eick M. J., Grossl P., and Sparks D. L. (1997) Arsenate and chromate retention mechanisms on goethite. 1. Surface Structure. *Environ. Sci. Technol.* **31,** 315–320.

Ferris F. G., Beveridge T. J., and Fyfe W. S. (1986) Iron-silica crystallite nucleation by bacteria in a geothermal sediment. *Nature* **320,** 609–611.

Ferris M. J., Muyzer G., and Ward D. M. (1996) Denaturing gradient gel electrophoresis profiles of 16S rRNA-defined populations inhabiting a hot spring microbial mat community. *Appl. Environ. Microbiol.* **62,** 340–346.

Ford R. G. (2002) Rates of hydrous ferric oxide crysallization and the influence on coprecipitated arsenate. *Environ. Sci. Technol.* **36,** 2459–2463.

Fournier R. O. (1989) Geochemistry and dynamics of the Yellowstone National Park hydrothermal system. *Ann. Rev. Planet. Sci.* **17,** 13–53.

Franke I. H., Fegan M., Hayward C., Leonard G., Stackebrandt E., and Sly L. I. (1999) Description of *Gluconacetobacter sacchari* sp. nov., a new species of acetic acid bacterium isolated from the leaf sheath

of sugar cane and from the pink sugar cane mealy bug. *Int. J. Syst. Bacteriol.* **49,** 1681–1693.

Fuchs T., Huber H., Burggraf S., and Stetter K. O. (1996) 16S rDNA-based phylogeny of the archaeal order sulfolobales and reclassification of *Desulfurolobus ambivalens* as *Acidianus ambivalens* comb. nov. *System. Appl. Microbiol.* **19,** 56–60.

Ghiorse W. C. (1984) Biology of iron-and manganese-depositing bacteria. *Ann. Rev. Microb.* **38,** 515–550.

Gihring T. M., Druschel G. K., McCleskey R. B., Hamers R. J., and Banfield J. F. (2001) Rapid arsenite oxidation by *Thermus aquaticus* and *Thermus thermophilus*: Field and laboratory investigations. *Environ. Sci. Technol.* **35,** 3857–3862.

Hawthorne F. C. (1976) Hydrogen positions in scorodite. *Acta Cryst. B Struct. Sci.* **32,** 2891–2892.

Inskeep W. P., McDermott T. R., and Fendorf S. (2002) Arsenic (V)/(III) cycling in soils and natural waters: Chemical and microbiological processes. In *Environmental Chemistry of Arsenic* (ed. W. T. Frankenberger, Jr.), pp. 183–215. Marcel Dekker.

Jackson C. R., Langner H. W., Donahoe-Christiansen J., Inskeep W. P., and McDermott T. R. (2001) Molecular analysis of microbial community structure in an arsenite-oxidizing acidic thermal spring. *Environ. Microbiol.* **3,** 532–542.

Karl D. M., McMurtry G. M., Malahoff A., and Garcia M. O. (1988) Loihi Seamount, Hawaii: A mid-plate volcano with a distinctive hydrothermal system. *Nature* **335,** 532–535.

Konhauser K. O. (1998) Diversity of bacterial iron mineralization. *Earth Sci. Rev.* **43,** 91–121.

Konhauser K. O. and Ferris F. G. (1996) Diversity of iron and silica precipitation by microbial mats in hydrothermal waters, Iceland: Implications for Precambrian iron formations. *Geology* **24,** 323–326.

Lane D. J., Harrison A. P., Jr., Stahl D., Pace B., Giovannoni S. J., Olsen G. J., and Pace N. R. (1992) Evolutionary relationships among sulfur- and iron- oxidizing eubacteria. *J. Bacteriol.* **174,** 269–278.

Langner H. W., Jackson C. R., McDermott T. R., and Inskeep W. P. (2001) Rapid oxidation of arsenite in a hot spring ecosystem, Yellowstone National Park. *Environ. Sci. Technol.* **35,** 3302–3309.

Leblanc M., Achard B., Ben Othman D., Luck J. M., Bertrand-Sarfati J., and Personné J. C. (1996) Accumulation of arsenic from acidic mine waters by ferruginous bacterial accretions (stromatolites). *Appl. Geochem.* **11,** 541–554.

Loeppert R. H. and Inskeep W. P. (1996) Iron. In *Methods of Soil Analysis, Part 3, Chemical Methods* (ed. D. L. Sparks), pp. 639–664. SSSA book series no. 5. Soil Science Society of America and American Society of Agronomy.

MacArthur J. M., Ravenscroft P., Safiulla S., and Thirwall M. F. (2001) Arsenic in groundwater: Testing pollution mechanisms for sedimentary aquifers in Bangladesh. *Water Resour. Res.* **37,** 109–117.

Macur R. E. (2004) Linking microbial populations and geochemical processes in soils, mine tailings and geothermal environments. Ph.D. dissertation, Montana State University, 147 pages.

Manceau A. (1995) The mechanism of anion adsorption on Fe oxides: Evidence for the bonding of arsenate tetrahedra on free Fe(O, OH)6 edges. *Geochim. Cosmochim. Acta* **59,** 3647–3653.

Manceau A. and Drits V. A. (1993) Local structure of ferrihydrite and feroxyhite by EXAFS spectroscopy. *Clay Min.* **28,** 165–184.

Manning B. A., Fendorf S. E., and Goldberg S. (1998) Surface structures and stability of arsenic(III) on geothite: Spectroscopic evidence for inner-sphere complexes. *Environ. Sci. Technol.* **32,** 2383–2388.

Morin G., Juillot F., Casiot C., Bruneel O., Personné J., Elbaz-Poulichet F., Leblanc M., Ildefonse P., and Calas G. (2003) Bacterial formation of tooeleite and mixed arsenic(III) or arsenic(V)-iron (III) gels in the Carnoulès acid mine drainage, France: A XANES, XRD, and SEM study. *Environ. Sci. Technol.* **37,** 1705–1712.

Newman D. K. and Banfield J. F. (2002) Geomicrobiology: How molecular-scale interactions underpin biogeochemical systems. *Science* **296,** 1071–1077.

Pichler T., Veizer J., and Hall G. E. M. (1999) Natural input of As into a coral-reef ecosystem by hydrothermal fluids and its removal by Fe(III) oxyhydroxides. *Environ. Sci. Technol.* **33,** 1373–1378.

Rancourt D. G., Fortin D., Pichler T., Thibault PJ., Lamarche G., Morris R. V., and Mercier P. H. J. (2001) Mineralogy of a natural As-rich hydrous ferric oxide coprecipitate formed by mixing of hydrothermal fluid and seawater: Implications regarding surface complexation and color banding in ferrihydrite deposits. *Am. Mineral.* **86,** 834–851.

Raven K. P., Jain A., and Loeppert R. H. (1998) Arsenite and arsenate adsorption on ferrihydrite: Kinetics, equilibrium, and adsorption envelopes. *Environ. Sci. Technol.* **32,** 344–349.

Reysenbach A.-L. and Shock E. (2002) Merging genomes with geochemistry in hydrothermal ecosystems. *Science* **296,** 1077.

Sako Y., Nakagawa S., Takai K., and Horikoshi K. (2003) *Marinithermis hydrothermalis* gen. nov., sp. nov., a strictly aerobic, thermophilic bacterium from a deep-sea hydrothemal vent chimney. *Int. J. Sys. Evol. Microbiol.* **53,** 59–65.

Salmassi T. M., Venkateswaren K., Satomi M., Nealson K. H., Newman D. K., and Hering J. G. (2002) Oxidation of arsenite by *Agrobacterium albertimagni*, AOL15, sp. nov., isolated from Hot Creek, California. *Geomicrobiol. J.* **19,** 53–66.

Smith D. K. (1998) Opal, cristobalite, and tridymite: Noncrystallinity versus crystallinity, nomenclature of the silica minerals and bibliography. *Powder Diffraction* **13,** 2–19.

Spurr A. R. (1969) A low-viscosity epoxy resin embedding medium for electron microscopy. *J. Ultrastructure Res.* **26,** 31–43.

Sun X. and Doner H. E. (1998) Adsorption and oxidation of arsenite on goethite. *Soil Sci.* **163,** 278–287.

Takai K. and Sako Y. (1999) A molecular view of archaeal diversity in marine and terrestrial hot water environments. *FEMS Microbiol Ecol.* **28,** 177–188.

To T. B., Nordstrom D. K., Cunningham K. M., Ball J. W., and McCleskey R. B. (1999) New method for the direct determination of dissolved Fe(III) concentration in acid mine waters. *Environ. Sci. Technol.* **33,** 807–813.

Vetriani C., Jannasch H. W., MacGregor B. J., Stahl D. A., and Reysenbach A. L. (1999) Population structure and phylogenetic characterization of marine benthic Archaea in deep-sea sediments. *Appl. Environ. Microbiol.* **65,** 4375–4384.

Ward D. M. (1998) A natural species concept for prokaryotes. *Curr. Opin. Microbiol.* **1,** 271–277.

Waychunas G. A., Rea B. A., Fuller C. C., and Davis J. A. (1993) Surface chemistry of ferrihydrite: Part 1. EXAFS studies of the geometry of coprecipitated and adsorbed arsenate. *Geochim. Cosmochim. Acta* **57,** 2251–2269.

Waychunas G. A., Davis J. A., and Fuller C. C. (1995) Geometry of sorbed arsenate on ferrihydrite and crystalline FeOOH: Re-evaluation of EXAFS results and topological factors in predicting sorbate geometry, and evidence for monodentate complexes. *Geochim. Cosmochim. Acta* **59,** 3655–3661.

Wilkie J. A. and Hering J. G. (1998) Rapid oxidation of geothermal arsenic(III) in streamwaters of the Eastern Sierra Nevada. *Environ. Sci. Technol.* **32,** 657–662.

Xu Y., Schoonen M. A. A., Nordstrom D. K., Cunningham K. M., and Ball J. W. (1998) Sulfur geochemistry of hydrothermal waters in Yellowstone National Park: I. The origin of thiosulfate in hot spring waters. *Geochim. Cosmochim. Acta* **62,** 3729–3743.

Zabinsky S. I., Rehr J. J., Ankudinov A., Albers R. C., and Eller M. J. (1995) Multiple scattering calculations of x-ray absorption spectra. *Phys. Rev.* **52,** 2995–3009.

Zobrist J., Dowdle P. R., Davis J. A., and Oremland R. S. (2000) Mobilization of arsenite by dissimilatory reduction of adsorbed arsenate. *Environ. Sci. Technol.* **34,** 4747–475.